PAPER • OPEN ACCESS

Optically-detected spin-echo method for relaxation times measurements in a Rb atomic vapor

New Journal of Physics
The open access journal at the forefront of physics

Deutsche Physikalische Gesellschaft DPG
IOP Institute of Physics

Published in partnership with: Deutsche Physikalische Gesellschaft and the Institute of Physics

OPEN ACCESS

RECEIVED
21 December 2016

REVISED
18 April 2017

ACCEPTED FOR PUBLICATION
17 May 2017

PUBLISHED
26 June 2017

PAPER

Optically-detected spin-echo method for relaxation times measurements in a Rb atomic vapor

M Gharavipour[1,3], C Affolderbach[1], F Gruet[1], I S Radojičić[2], A J Krmpot[2], B M Jelenković[2] and G Mileti[1,3]

[1] Laboratoire Temps-Fréquence (LTF), Institut de Physique, Université de Neuchâtel, Neuchâtel CH-2000, Switzerland
[2] Institute of Physics Belgrade, University of Belgrade, Pregrevica 118, 11080 Belgrade, Serbia
[3] Authors to whom any correspondence should be addressed

E-mail: mohammadreza.gharavipour@unine.ch **and** gaetano.mileti@unine.ch

Keywords: relaxation times, vapor cell atomic clock, spin-echo, optical detection, Ramsey scheme

Abstract

We introduce and demonstrate an experimental method, optically-detected spin-echo (ODSE), to measure ground-state relaxation times of a rubidium (Rb) atomic vapor held in a glass cell with buffer-gas. The work is motivated by our studies on high-performance Rb atomic clocks, where both population and coherence relaxation times (T_1 and T_2, respectively) of the 'clock transition' ($5^2S_{1/2}$ $|F_g = 1, m_F = 0\rangle \leftrightarrow |F_g = 2, m_F = 0\rangle$) are relevant. Our ODSE method is inspired by classical nuclear magnetic resonance spin-echo method, combined with optical detection. In contrast to other existing methods, like continuous-wave double-resonance (CW-DR) and Ramsey-DR, principles of the ODSE method allow suppression of decoherence arising from the inhomogeneity of the static magnetic field across the vapor cell, thus enabling measurements of intrinsic relaxation rates, as properties of the cell alone. Our experimental result for the coherence relaxation time, specific for the clock transition, measured with the ODSE method is in good agreement with the theoretical prediction, and the ODSE results are validated by comparison to those obtained with Franzen, CW-DR and Ramsey-DR methods. The method is of interest for a wide variety of quantum optics experiments with optical signal readout.

1. Introduction

Alkali atomic vapors are widely used in many types of high-resolution atomic physics experiments like nuclear magnetic resonance (NMR) [1] and precision measurements in applications such as optical magnetometry [2], vapor cell atomic frequency standards [3, 4], quantum entanglement and information storage [5], miniature atomic clocks [6], navigation systems [7–9], spin squeezing [10]. All these applications rely on long-lived ground-state spin-polarization of the alkali vapor in the cell [11]. Particularly in the vapor-cell atomic clocks, the clock stability critically depends on width and contrast of the atomic resonance line. The resonance linewidth is determined by various parameters, and ultimately, by the relaxation processes occurring in the cell. Like in NMR, alkali atoms in the vapor cell may lose their polarization due to various types of collisions, interactions with electro-magnetic fields, and also due to inhomogeneity of the static magnetic field.

Studies of relaxation processes in various spin-polarized systems have a long-standing history of more than 70 years. In the case of atomic relaxations in alkali vapors, Franzen presented the 'relaxation in the dark' method [12] in 1959 and measured the population relaxation time of optically-pumped Rb atoms in the vapor cell. Franzen's method has been modified and used by other groups to determine both population and coherence relaxation times in Rb or Cs wall-coated vapor cells [13–16]. Moreover, methods of nonlinear magneto-optical rotation [11, 17], ground-state Hanle effect [18, 19] and optically detected magnetic resonance [19, 20] were employed to measure the hyperfine and the Zeeman relaxation times in wall-coated or in buffer-gas alkali vapor cells. Various modified NMR spin-echo techniques [21] have been studied both theoretically and experimentally for solid-state systems to extend the coherence time [22, 23]. Similar techniques like dynamical decoupling approach [24, 25] and gradient echo memory [26] applied in quantum memory studies aim for example to

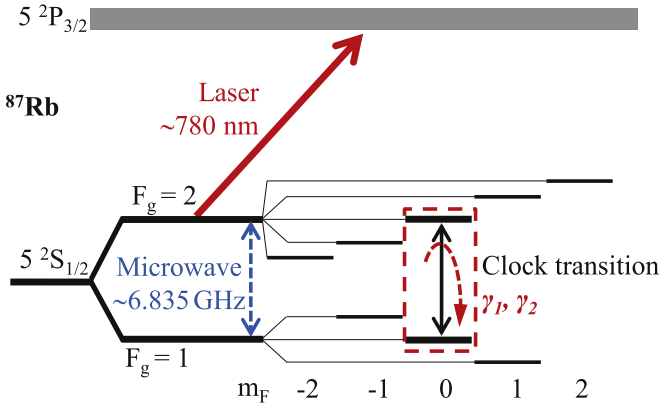

Figure 1. Atomic level scheme of ^{87}Rb. The optical pumping with the laser at 780 nm creates a population imbalance between two ground states $F_g = 1$ and $F_g = 2$ via excited-state $5^2P_{3/2}$. Due to Doppler and collisional broadening, the hyperfine levels of the excited-state are not resolved by the laser light. The clock transition ($5^2S_{1/2}|F_g = 1, m_F = 0\rangle \leftrightarrow |F_g = 2, m_F = 0\rangle$) is addressed by choosing appropriate microwave frequency. γ_1 and γ_2 are the population and coherence relaxations rates for the clock transition, respectively.

minimize the detrimental effect of inhomogeneous broadening on the coherence storage time of the quantum bit (qubit) or to use the artificially created broadening for storage of broad-band optical pulses without deterioration of the storage time [27–29].

In this paper, we present our 'optically-detected spin-echo' (ODSE) method to measure the relaxation times in a Rb vapor cell with buffer-gas. This method is a combination of Franzen [12], Ramsey-DR [16] and NMR spin-echo [21] techniques. We apply the ODSE method to our high-performance ^{87}Rb atomic frequency-standard setup presented in [30, 31] and show how to determine the intrinsic coherence relaxation time (T_2) specifically for the 'clock transition' ($5^2S_{1/2}|F_g = 1, m_F = 0\rangle \leftrightarrow |F_g = 2, m_F = 0\rangle$, see figure 1). Here we use the term 'intrinsic' to describe the relaxations that do not include any influence of any electro-magnetic field but are influenced only by the various types of collisions that depend on the cell design and the temperature [19] (see section 2). Gradients in the static magnetic field across the vapor cell are some of the main sources of the relaxation processes. Such induced relaxation processes may mask the real intrinsic relaxation times during measurements, thus hindering their precise determination. The ODSE method enables measurements that are free of the influence of the static magnetic field gradients.

In section 2 we briefly recall the theory of relaxation processes in a buffer-gas vapor cell [3], and use it to estimate the 'intrinsic' population and coherence relaxation times (T_1 and T_2 respectively) of the clock transition in our ^{87}Rb vapor cell. In section 3, we introduce the experimental setup which is basically a Rb atomic clock [30, 31]. Finally in section 4, we present the results of relaxation times measured in the same ^{87}Rb vapor cell by using ODSE, Franzen, continuous-wave double-resonance (CW-DR), and Ramsey-DR methods. The advantages and limitations of these methods are discussed.

2. Theory of relaxation processes in a buffer-gas vapor cell

Ultra-narrow signal linewidths employed in atomic precision experiments and instrumentations, such as atomic clocks, are ultimately limited by the relaxation processes in the atomic sample. For example in a Rb atomic clock, the frequency of a quartz oscillator is stabilized to the frequency of the ^{87}Rb hyperfine clock transition [32] observed in a Rb vapor cell. Rb atoms are optically pumped with a laser to create a population imbalance and microwave interrogation creates a coherence between the two ground states $F_g = 1$ and $F_g = 2$ of ^{87}Rb atoms. Due to the relaxation processes, this population imbalance and coherence may be destroyed and the prepared Rb atoms lose their polarization. The dynamics of this process is characterized by the relaxation times on the atomic levels. The two parameters of longitudinal relaxation rate γ_1 and transverse relaxation rate γ_2—which are inverse of the relaxation times T_1 and T_2, respectively—describe the population and coherence relaxations for the clock transition, respectively (see figure 1).

We use the well-known relaxation theory [3] and the experimentally-determined parameters presented in [3] to estimate approximately γ_1 and γ_2 for our ^{87}Rb vapor cell. Collisions of polarized ^{87}Rb atoms with the cell walls, with buffer-gas particles and with other Rb atoms—the latter is known as spin-exchange—are the sources of relaxation processes occurring in a vapor cell. The total intrinsic population and coherence relaxation rates, γ_i (here and in the following index i stands for 1 and 2 for the population and coherence, respectively), are equal to

Table 1. Calculated intrinsic relaxation rates/times in Rb vapor cell, at $T = 336$ K.

	γ_1 (s^{-1})	γ_2 (s^{-1})
Buffer gas collisions (γ_{iBG})	12	79
Diffusion to cell walls (γ_{iW})	26	25
Spin-exchange (γ_{iSE})	185	116
Total rates	223	220
Calculated relaxation times (ms)	$T_1 = 4.5\,(3)$	$T_2 = 4.5\,(3)$

the sum of the three relaxation processes induced by the cell walls γ_{iW}, the buffer-gas γ_{iBG} and spin-exchange γ_{iSE}.

The presence of a buffer gas in the cell reduces the rate of depolarizing collisions between Rb atoms and the cell walls. Therefore, relaxation rates γ_{iW}, due to collisions of Rb atoms with the cell-walls, depend on the cell dimensions, cell temperature T and the total buffer-gas pressure, P, in the cell. In lowest order diffusion approximation, it is described by [3]:

$$\gamma_{iW} = ((2.405/a)^2 + (\pi/L)^2) D_i (P_0/P), \tag{1}$$

where $a = 1.25$ cm and $L = 2.5$ cm are the radius and length of our cylindrical ^{87}Rb vapor cell, respectively. D_i is the diffusion constant of Rb atoms in the buffer-gas particles of interest which is proportional to $T^{3/2}$, P_0 is the standard atmospheric pressure (1013.25 mbar) and P is about 33 mbar in our vapor cell.

Rb atoms also collide with the buffer-gas molecules in the vapor cell, which changes the electron density at the Rb nucleus and results in a change of hyperfine coupling in the Rb atoms [33]. The resulting buffer-gas relaxation rate γ_{iBG} is described as:

$$\gamma_{iBG} = L_0 \overline{v_r} \sigma_i (P/P_0), \tag{2}$$

where $L_0 = 2.686\,7774\,(47) \times 10^{25}$ m^{-3} at 0 °C is Loschmidt's constant, $\overline{v_r}$ is the mean relative velocity between a ^{87}Rb atom and a buffer-gas particle, and σ_i are the collisional cross-sections between colliding particles responsible for population and coherence relaxations. The temperature dependence of the above equation appears in the average relative velocity $\overline{v_r} = (8k_B T/\pi\mu)^{1/2}$ where k_B is the Boltzmann constant and μ is the reduced mass of the colliding particles (here Rb and buffer-gas atoms).

Note that in the case of anti-relaxation wall-coated cells the relaxation processes as described by equations (1) and (2) do not apply and the relaxation rates are instead governed by the properties and the quality (such as purity and coverage) of the coating [34–36]. Such wall-coated cells are however not considered in this study.

Collisions between Rb atoms in the vapor cell result in de-coherence due to spin exchange. The resulting population γ_{1SE} and coherence γ_{2SE} broadening are described by:

$$\gamma_{1SE} = n \overline{v_s} \sigma_{SE}, \tag{3}$$

$$\gamma_{2SE} = \gamma_{1SE} (6I + 1)/(8I + 4), \tag{4}$$

respectively, where n is the number density of the Rb vapor, $\overline{v_s}$ is the average relative velocity between two ^{87}Rb atoms and $\sigma_{SE} = 1.6 \times 10^{-18}$ m^2 is the spin-exchange cross section. I is the nuclear spin and for ^{87}Rb is equal to 3/2.

The total expected relaxation rates in our cell are given by:

$$\gamma_i = \gamma_{iBG} + \gamma_{iW} + \gamma_{iSE}. \tag{5}$$

All these contributions to the intrinsic population and coherence relaxation rates are listed in table 1. They were calculated from equations (1)–(4) for the clock transition in our ^{87}Rb vapor cell using experimentally measured parameters for D_i and σ_i taken from [3]. Finally, both intrinsic relaxation times for the clock transition are calculated to be $T_1 \approx T_2 = 4.5$ ms. We note that the reported literature values for D_i and σ_i show considerable scatter, which results in a total uncertainty of 7% for both intrinsic T_1 and T_2 [12, 37–39].

In addition to the various presented types of collisions of the polarized Rb atoms in the vapor cell, their interactions with other electromagnetic fields may also be interpreted as sources of relaxations. The electromagnetic fields present in our atomic clock are the optical and the microwave fields that are used to prepare, drive and detect the resonance [30, 32] and the static magnetic field applied to lift the Zeeman degeneracy. The latter may have some residual inhomogeneity across the vapor cell. In a microscopic view, Rb atoms can move in the vapor cell and—due to the field inhomogeneity—they may experience various static magnetic fields. This effect introduces additional dephasing [40] which results in a decrease of the measured

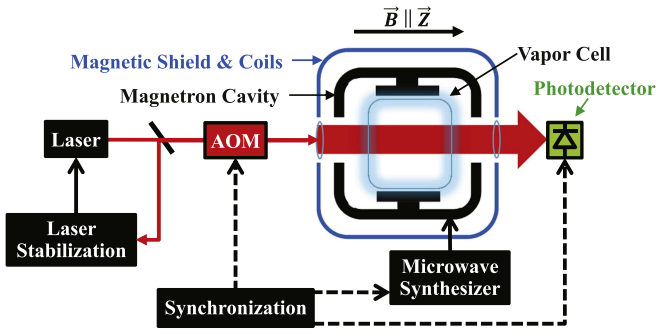

Figure 2. Schematic of the experimental setup. The static magnetic field $\vec{B}$ is oriented parallel to the cell's symmetry axis and the laser propagation vector ($\vec{Z}$ direction). The cylindrical vapor cell has both diameter and length of 25 mm. (AOM—acousto-optical-modulator.)

coherence relaxation time depending on the method (see section 4). In NMR, the overall coherence relaxation time T_2^* due to the field inhomogeneity is given by [41]:

$$T_2^{*-1} = T_2^{-1} + \eta G^2, \tag{6}$$

where, T_2 is the intrinsic coherence relaxation time, G is the local gradient of the static magnetic field and η is a proportionality factor depending on atomic and experimental parameters.

In this study, we determine the coherence time T_2^* by using CW-DR and Ramsey-DR schemes (sections 4.2 and 4.3, respectively), while with ODSE method the intrinsic coherence relaxation time T_2 is obtained (section 4.4).

The system studied here is an alkali vapor cell with relatively high buffer-gas pressure, where the Rb atoms are effectively localized to a few micrometers over the measurement timescales. Due to this localization, the sample shows inhomogeneous shifts and broadenings because of the inhomogeneity of external fields [42]. This is fundamentally different from the case of anti-relaxation wall-coated cells without buffer gas where the atoms move freely through the entire cell volume and experience only homogeneous shifts and broadenings as well as narrowing [43].

3. Experimental setup

Figure 2 shows the schematics of our experimental setup, basically a Rb atomic clock, whose details were previously presented in [30, 31]. It consists of three main parts: (1) the physics package containing the microwave cavity and the vapor cell, (2) the compact frequency-stabilized laser head (LH), and (3) the microwave synthesizer. The physics package contains the in-house-made cylindrical glass cell with both diameter and length of 25 mm. The cell contains isotopically enriched ^{87}Rb and a mixture of Argon and Nitrogen as buffer gases. The vapor cell is placed in a compact magnetron-type microwave cavity which resonates at the ^{87}Rb clock transition frequency of $\approx$6.835 GHz, with a TE_{011}-like field-mode geometry [44]. A magnetic coil placed around the cavity generates a static magnetic field oriented parallel to the cell's symmetry axis and the laser propagation vector ($\vec{Z}$ direction) to lift the degeneracy of ^{87}Rb hyperfine ground states into their respective Zeeman levels. The laser is a distributed-feedback laser diode emitting at 780 nm frequency stabilized on Rb D2 sub-Doppler absorption lines using a compact (1.4 cm^3) magnetically-shielded and thermally-controlled ^{87}Rb evacuated cell. An acousto-optical-modulator (AOM) is implemented in the LH and serves as a switch to control the duration and intensity of the laser pulses [45]. The AOM has the fall and rise times <5 μs. The microwave synthesizer is used to generate the $\approx$6.835 GHz radiation for ^{87}Rb clock transition with a resolution below 1 μHz, and also controls the optical and microwave pulse sequences with a timing resolution at the level of 2 μs, as used in the pulsed schemes [46]. All pulse durations and synchronization in the pulsed schemes are referenced to the high-stability quartz oscillator of the atomic clock setup, thus assuring a timing accuracy far below the nanosecond level over the duration of the pulse sequences employed (for typical pulse sequences, see sections 4.1, 4.3, and 4.4).

4. Characterization methods and results

We apply four methods, Franzen, CW-DR, Ramsey-DR and ODSE to measure the relaxation times in the buffer-gas ^{87}Rb vapor cell. The CW-DR and Ramsey-DR schemes were previously also used for analyses from a

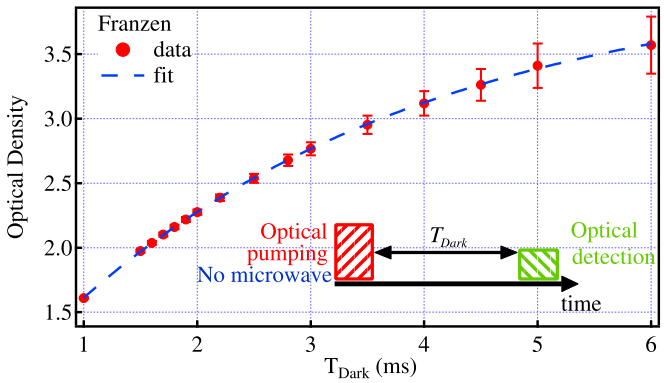

Figure 3. Optical density of the vapor cell in the Franzen scheme with the pump and probe pulse duration of 1 ms and 0.1 ms, respectively. The frequency of the laser pump and probe pulses are the same but the intensity of the optical detection pulse is about 100 times weaker than the intensity of the optical pumping pulse. Solid red circles are the experimental data with corresponding error bars and blue dashed curve is a fit based on equation (8). Error bars are dominated by technical noise and increase with increasing T_{Dark} due to decreasing transmitted intensity, I_t. Inset: timing sequence of the Franzen scheme.

metrological point of view including the short- and long-term frequency stability of our Rb atomic clock [47]. Franzen, Ramsey-DR and ODSE methods operate in pulse mode. In these three pulsed methods, first an optical pumping laser pulse creates a population imbalance by depopulating the ^{87}Rb $F_g = 2$ and filling the $F_g = 1$ ground state in the vapor cell (see figure 1). In the cases of Ramsey-DR and ODSE methods, optical pumping is followed by series of $\pi/2$ and/or π microwave pulses that create/modify coherence between the ground states. Finally—in all three pulse schemes—a laser probe pulse with the same frequency as during the optical pumping pulse is used to measure the optical density (OD) on the transition starting from $F_g = 2$ state by using a photodetector. To avoid re-pumping, this probe pulse has an approximately 100 times weaker intensity than the pump pulse. The variation of the OD as a function of time gives information about the population and/or coherence relaxation times. OD is defined to be the ratio of the incident I_0 and transmitted I_t laser probe pulse intensities:

$$\mathrm{OD} = -\ln(I_t/I_0). \tag{7}$$

In the pulsed schemes, the laser probe pulse used for the detection does not resolve the atomic excited state because all the optical transitions to this $5^2P_{3/2}$ state are overlapped within Doppler linewidth. Furthermore, the clock transition cannot be addressed selectively by the laser alone either, because both the intrinsic transition linewidth and the Doppler linewidth are much larger than the Zeeman splitting in the $5S_{1/2}$ ground state. Hence, in these pulsed schemes, we can only address the population relaxation time between *all* m_F levels of the ground stats $F_g = 1$ and $F_g = 2$ *simultaneously* (and not the clock transition only) which we write T_1' throughout this article. In Ramsey-DR and ODSE methods the frequency of the microwave field selects a particular hyperfine transition, which allows measuring its coherence relaxation time referring to the two involved m_F states only.

In the case of the CW-DR scheme, the linewidth of the resonance signal can be used to extract the coherence relaxation time for the clock transition. Also in the CW-DR scheme, the microwave frequency selects the specific Zeeman sublevels of interest. In all the above methods, no Doppler broadening occurs on the microwave transition, due to Dicke narrowing [43].

4.1. Franzen scheme

Franzen's well-known scheme of relaxation in the dark [12] for measuring population relaxation time is an all optical method, with absence of any microwave pulse. The timing sequence of the Franzen scheme is shown in inset in figure 3. First, a population imbalance is created between the ground states of ^{87}Rb atoms with the optical pumping. Then during the dark time T_{Dark}, the laser beam is switched off and the hyperfine population imbalance relaxes towards the thermal equilibrium. Finally, with a second laser pulse the sample's OD is probed which is a measure of the atomic population in $F_g = 2$. Figure 3 shows the experimentally obtained OD when T_{Dark} is varied, with the pump and probe pulse duration of 1 ms and 0.1 ms, respectively. By increasing the dark time, more atoms decay from $F_g = 1$ to $F_g = 2$ which results in increasing the OD. The data for the measurement is fitted with the equation:

$$\mathrm{OD} = A - B\exp(-T_{\mathrm{Dark}}/T_1'^{\mathrm{Franzen}}), \tag{8}$$

where A, B and $T_1'^{\mathrm{Franzen}}$ are the fitting parameters. As mentioned above, with this scheme only the population relaxation time of all m_F levels simultaneously is measured, which is determined as $T_1'^{\mathrm{Franzen}} = 3.23\,(6)$ ms from

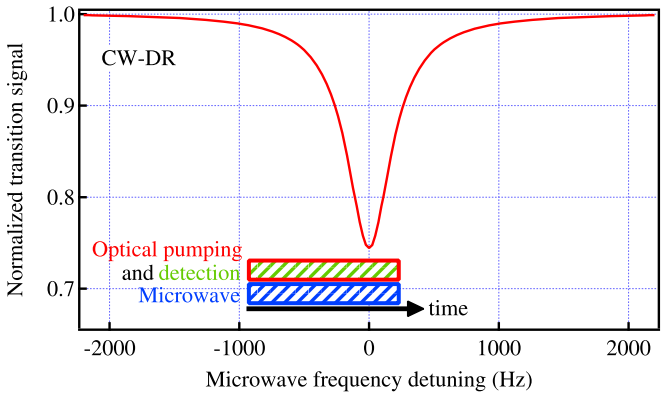

Figure 4. Typical DR signal in the CW-DR scheme when the microwave and laser input powers to the cavity and the cell are 0.45 μW and 125 μW, respectively. Inset: timing sequence of the CW-DR scheme.

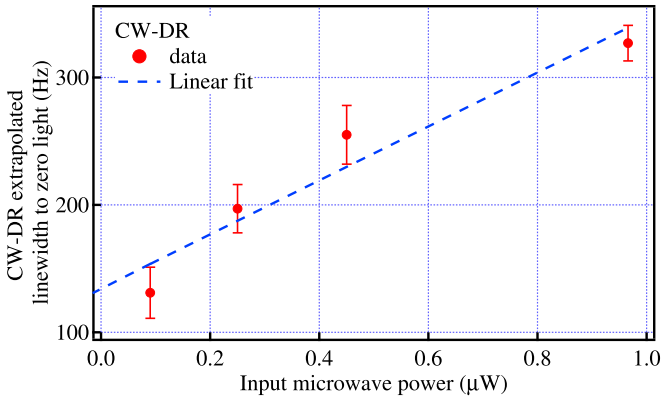

Figure 5. Extrapolation of the DR signal linewidth to zero optical and microwave powers. Solid red circles are the linewidths obtained by extrapolation to zero laser power and the blue dashed line is the linear fit of the data.

equation (8). This result did not change significantly when the measurement was repeated with the pump and probe pulse durations varied by $\pm 50\%$.

4.2. CW-DR scheme

In the case of CW-DR scheme [30], the laser optically pumps the Rb atoms in the vapor, while simultaneously a microwave field near-resonant with the ^{87}Rb hyperfine clock transition is applied. The transmitted light signal as a function of microwave frequency is a measure of the atomic ground state polarization known as DR signal. Figure 4 shows a typical DR signal which is obtained when the microwave frequency is scanned near resonance with 0.45 μW input power to the cavity and with 125 μW optical power to the cell. The linewidth of the DR signal is a measure of the coherence relaxation rate [32], but is additionally increased by optical and microwave power broadenings. To correct for this power broadening, the intrinsic DR signal linewidth, $\Delta\nu_{1/2}$, is determined by extrapolating the measured linewidth to zero with respect to both the optical and microwave powers, figure 5. By using this method, a coherence relaxation time for the clock transition, which is selectively driven by the applied microwave, is found to be $T_2^{*\text{CW-DR}} = (\pi\Delta\nu_{1/2})^{-1} = 2.4\ (4)$ ms [3]. However, this $T_2^{*\text{CW-DR}}$ is significantly smaller than the predicted intrinsic T_2 from table 1. This can be attributed to uncertainties in the extrapolations and to additional relaxation due to gradients of the static magnetic field in the vapor cell which are well-known from NMR [40, 41].

4.3. Ramsey-DR scheme

In the Ramsey-DR scheme [48, 49], the three steps of optical pumping, microwave interrogation and optical detection are separated in time, see inset in figure 6. First, during the optical pumping a strong laser pulse creates a population imbalance between the two ground-state sublevels of ^{87}Rb. The optical pumping pulse has an input power to the vapor cell on the level of 14 mW and a duration of 0.4 ms. After this pumping pulse, in absence of light, two coherent $\pi/2$ microwave pulses are applied that are separated by the Ramsey time T_R. Both microwave

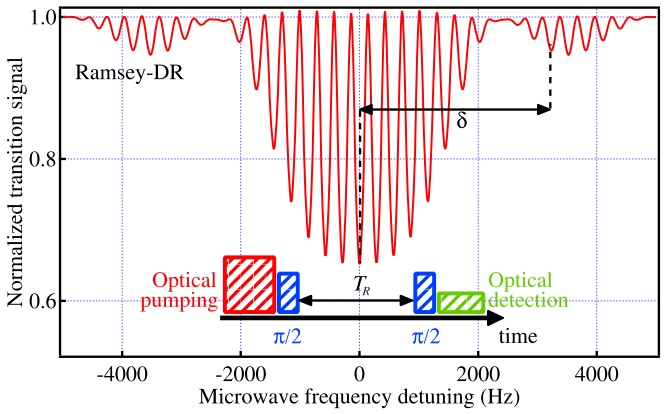

Figure 6. Typical Ramsey fringes obtained when $T_R = 3$ ms. Inset: timing sequence of the Ramsey-DR scheme.

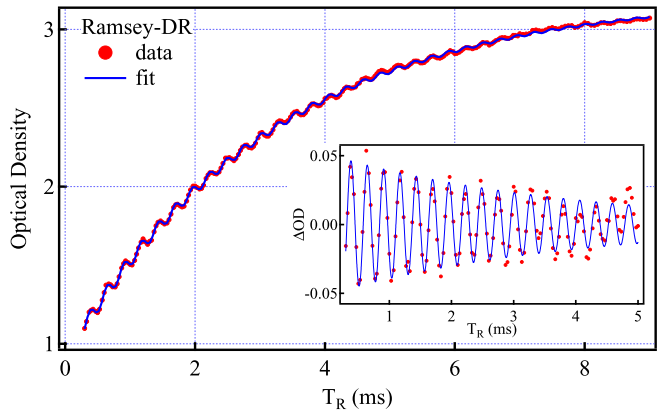

Figure 7. Optical density of the vapor cell in the Ramsey-DR scheme. Solid red circles are the experimental data and blue dashed curve is a fit based on equation (9). Inset: plot of the third term of equation (9).

pulses have the same duration of 0.4 ms, the same amplitude corresponding to a power of −18.2 dBm injected to the cavity and the same microwave frequency. The amplitude and duration of the $\pi/2$ microwave pulses in our Rb atomic clock were optimized according to the Rabi oscillation method presented in [50].

On the atomic level, the first $\pi/2$ microwave pulse creates a coherent superposition of the two hyperfine $m_F = 0$ states involved in the clock transition. During the Ramsey time, atoms evolve freely at the Larmor frequency. The second resonant microwave pulse converts the accumulated atomic phase into a population difference between the hyperfine states. Finally, in the last sequence the optical detection takes place with the laser. The laser frequency is the same for both optical pumping and detection steps, but the laser intensity is about 100 times weaker during the detection. In the Ramsey-DR scheme, the optical detection pulse duration is 0.7 ms [51] which results in an overall duration of one complete interrogation cycle of the scheme equal to $T_R + 1.9$ ms.

Figure 6 shows typical detected Ramsey fringes obtained by varying the microwave pulse frequency around the clock transition frequency, here for a Ramsey time of $T_R = 3$ ms. The OD of the Rb vapor is recorded for various values of T_R, with the microwave detuned from the clock transition by a fixed detuning δ (see figure 6) [16]. Figure 7 shows the recorded OD as a function of Ramsey time when the cavity is placed in a static magnetic field of 40 mG and the frequency of the microwave field is detuned from the resonance by $\delta = 3.8$ kHz. The data is fitted with the function [16]:

$$\mathrm{OD} = A - B\exp(-T_R/T_1'^{\mathrm{Ramsey}}) + C\exp(-T_R/T_2^{*\mathrm{Ramsey}})\sin(2\pi\delta T_R + \varphi), \quad (9)$$

where A, B, C, $T_1'^{\mathrm{Ramsey}}$, $T_2^{*\mathrm{Ramsey}}$, δ and φ are the fitting parameters. The fit gives the relaxation times with uncertainties $T_1'^{\mathrm{Ramsey}} = 3.20\,(1)$ ms and $T_2^{*\mathrm{Ramsey}} = 3.95\,(25)$ ms. Inset of figure 7 is the plot of the third term of equation (9) which shows the Ramsey oscillations in better contrast than the OD plot in figure 7.

In this method, like in the Franzen method, the $T_1'^{\mathrm{Ramsey}}$ is a measurement of the population relaxation time for all m_F levels confounded and it is consistent with $T_1'^{\mathrm{Franzen}}$. However in contrast to the $T_1'^{\mathrm{Ramsey}}$ population

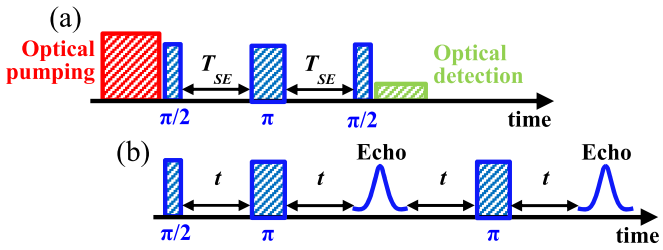

Figure 8. Timing sequences of: (a) ODSE scheme. (b) Classical spin-echo scheme.

relaxation time, $T_2^{*\text{Ramsey}}$ refers to the coherence relaxation time specific for the clock transition alone [16]. It is longer than T_2 from CW-DR method, but this $T_2^{*\text{Ramsey}}$ is still significantly shorter than the predicted coherence relaxation time ($T_2 = 4.5$ ms) from section 2. A likely reason for this can be the presence of the inhomogeneity of the static magnetic field inside our vapor cell that motivated us to propose our ODSE method to suppress this effect and measure the intrinsic T_2 (see section 4.4). Although, we note that such static magnetic field gradients are generally small across the vapor cell in our atomic clock, for example on the order of 4% in a similar physics package (see [52]).

In addition to the relaxation times, the microwave detuning from the resonance—which is given by the Ramsey oscillations—is obtained from the fit to equation (9) to be $\delta = 3.8 \pm 0.003$ kHz which is in excellent agreement with the measurement conditions.

4.4. ODSE scheme

In order to suppress coherence relaxation due to static magnetic field gradients (see section 2), we propose the new scheme of ODSE. The ODSE method is inspired by the NMR spin-echo method presented by Hahn [21] which is used to narrow the resonance line broadening in inhomogeneous static magnetic fields.

In classical NMR spin-echo, a pickup coil is required to detect the magnetic moments' precession of the sample [40], which on one hand cannot easily be integrated into an atomic clock using a microwave cavity and on the other hand can collect noise from the cell and reemit the collected microwaves through the wires outside of the cell, thus producing additional noise. In the proposed ODSE method a photodetector is used to measure the OD in the vapor cell which is much more robust, reliable and does not feedback noise to the atoms, thus circumventing the problems existing in the standard method of detection using pickup coil.

In the Ramsey-DR scheme, after the first $\pi/2$ microwave pulse, because of the inhomogeneity of the static magnetic field, the atomic spins dephase at different rates and their coherence starts to decay which finally results in a shorter coherence relaxation time compared to the intrinsic T_2. To suppress this effect—like in NMR spin-echo—we apply a π microwave pulse added between the $\pi/2$ microwave pulses of the Ramsey-DR method and propose this resulting ODSE method for relaxation time measurements in an atomic vapor cell (see figure 8(a)). In the ODSE method, all the experimental conditions of optical pumping, optical detection and $\pi/2$ microwave pulses are the same as for the Ramsey-DR scheme (see section 4.3). The additional π pulse is separated from each of the two $\pi/2$ pulses by a dephasing time T_{SE} and has the same frequency and amplitude as the $\pi/2$ pulses, but its duration is two times longer so the duration of one complete cycle of ODSE scheme becomes $2T_{\text{SE}} + 2.7$ ms. The π pulse flips the direction of dephasing spins and reverses the spin phases (spin-flips). After some time equal to the dephasing time, T_{SE}, the dephased states are rephased at the instant of the second $\pi/2$ microwave pulse. Finally, the detection by the second $\pi/2$ pulse and the laser pulse destroys the atomic coherences so no more consecutive echoes (as observed in NMR, see figure 8(b)) can be detected. The OD of the vapor sample is recorded by varying the rephasing (and dephasing) time T_{SE}, with the same experimental conditions as in the case of Ramsey-DR scheme, i.e. a static magnetic field of 40 mG and microwave frequency detuning of $\delta = 3.8$ kHz from the clock transition. Like in the Ramsey-DR method, a trade-off exists for selecting δ in the ODSE method: for very small δ, big initial variations in I_t and thus in OD can be observed, but only few oscillations occur before they are damped away after about T_{R} or $T_{\text{SE}} \approx 2 \cdot T_2$. For very big δ on the other hand, many oscillations can be observed over this timescale but the maximum variation of I_t is small, which reduces the signal-to-noise ratio of the OD data.

The experimental data shown in figure 9 is fitted to the function:

$$\text{OD} = A - B\exp(-2T_{\text{SE}}/T_1{}'^{\text{ODSE}}) + C\exp(-2T_{\text{SE}}/T_2^{\text{ODSE}})\sin(4\pi\delta T_{\text{SE}} + \varphi), \tag{10}$$

where $A, B, C, T_1{}'^{\text{ODSE}}, T_2^{\text{ODSE}}, \delta$ and φ are the fitting parameters. The fit gives both the relaxation times of $T_1{}'^{\text{ODSE}} = 3.21\,(5)$ ms and $T_2^{\text{ODSE}} = 4.30\,(85)$ ms and $\delta = 3.8 \pm 0.005$ kHz. $T_1{}'^{\text{ODSE}}$ refers to the population relaxation time for the transitions between all m_F levels (like in the Franzen and Ramsey-DR methods). It shows

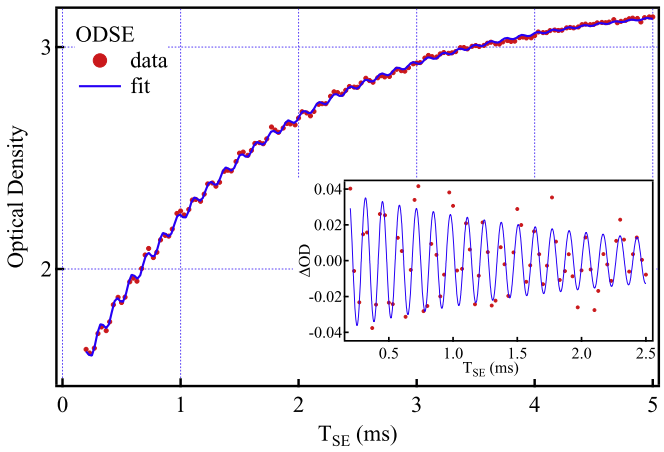

Figure 9. Optical density of the vapor cell in the ODSE scheme. Solid red circles are the experimental data and blue dashed curve is a fit based on equation (10). Inset: plot of the third term of equation (10).

a very good consistency with the obtained T_1' from Franzen and Ramsey-DR methods. The measured T_2^{ODSE} is in a good agreement with the predicted intrinsic coherence relaxation time T_2 (≈4.5 ms).

In our proof-of-principle experiment, the measured relaxation times in ODSE method have larger uncertainties (3–5 times) compared to the ones from the Ramsey-DR method. We attribute this phenomena to: (1) the ODSE signal has a lower amplitude than the Ramsey-DR signal which is due to the longer duration of one complete interrogation cycle (2.7 ms + $2T_{\mathrm{SE}}$ versus 1.9 ms + T_{R}), and (2) the residual instabilities of the microwave-synthesizer frequency over the entire measurement duration of about two hours may introduce additional noise on the signal (in Ramsey-DR and ODSE methods about 250 (figure 7) and 150 (figure 9) data points are presented, respectively).

To demonstrate the enhanced immunity of the ODSE method to inhomogeneity in the static magnetic field, the measurements were repeated with both Ramsey-DR and ODSE methods when the static magnetic field was doubled to 80 mG—resulting also in doubling of the static magnetic field gradient dominated by the geometry of the field coil—while all other parameters were kept unchanged. Under these conditions, with ODSE scheme the coherence relaxation time was measured to be $T_2^{\mathrm{ODSE}} = 4.26\,(80)$ ms which is consistent to better than 1% with the measured coherence relaxation time when the magnetic field was 40 mG. But in the case of the Ramsey-DR scheme at higher magnetic field, the coherence relaxation time was measured to be $T_2^{*\mathrm{Ramsey}} = 3.80\,(25)$ ms which is about 4% shorter compare to $T_2^{*\mathrm{Ramsey}} = 3.95\,(25)$ ms obtained with lower magnetic field and its gradient. This comparison shows that the ODSE scheme is a promising method to suppress the effect of inhomogeneity of the static magnetic field across the vapor cell, even in the case of our well-controlled clock physics package with its highly homogeneous magnetic field.

5. Conclusion

We have introduced and demonstrated the method of ODSE to determine the population relaxation time (for all m_F levels of the $F_g = 1$ and $F_g = 2$ ground states simultaneously) and the intrinsic coherence relaxation time, T_2, specifically for the clock transition in a thermal atomic vapor with buffer-gas in view of its application to atomic clocks. This method was compared to other well established Franzen, CW-DR and Ramsey-DR methods using the same ^{87}Rb vapor cell. The population relaxation time measured with the ODSE method was very consistent with the ones from Franzen and Ramsey-DR methods. In all those pulsed methods, the obtained population relaxation time measured for all m_F levels simultaneously (and not only for the clock transition). We have shown that the ODSE method suppresses coherence relaxation arising from gradients in the static magnetic field across the vapor cell and thus yields the intrinsic coherence relaxation time closer to the theoretically predicted T_2. In contrast, the measured coherence relaxation times by both CW-DR and Ramsey-DR methods were shorter than the predicted T_2, due to the inhomogeneity of the magnetic field.

Our proof-of-principle demonstrations shows that ODSE is a highly useful tool for measuring intrinsic relaxation rates in atomic vapors, independently of present magnetic field gradients. By measuring T_2 times with both the ODSE and Ramsey-DR schemes, it should also be possible to obtain experimental information on the magnetic field gradients across the atomic sample or vapor cell under study. Contrary to NMR spin-echo, our ODSE method does not need any pickup-coil but uses a photodetector to record the light absorbed in the vapor cell (OD), which is more robust and less noisy than detection in the radio-frequency or microwave regime.

Moreover, the photodetector can be conveniently placed outside the atomic vapor system under study—in our case outside the entire vapor-cell clock physics package—which makes the ODSE method an ideal candidate for characterizing relaxation times in atomic clocks with a cavity. While not covered by this present study, it would be of interest to study a potential extension of the ODSE technique to less localized atomic systems such as vapor cells without buffer-gas but equipped with an anti-relaxation wall coating. Similarly, the ODSE method is of high interest for characterizing relaxation rates in other quantum optics systems with optical readout, such as quantum information storage or processing [5, 53], cold-atom experiments [54], and other applications of quantum systems that rely on long-live atomic coherences.

Acknowledgments

This work was supported by the Swiss National Science Foundation (SNSF grants no. 140712 and 162346), the European Metrology Research Programme (EMRP project IND55-Mclocks), SNSF-Scopes project (152511) and Ministry of Education, Science and Technological Development of Republic Serbia (III 45016 and OI 171038) and COST Action 1403 Nanoscale Quantum Optics. The EMRP is jointly funded by the EMRP participating countries within EURAMET and the European Union. We thank A K Skrivervik and A Ivanov (both EPFL-LEMA) for their support on the microwave cavity, C Calosso (INRIM, Italy) for providing the microwave LO, W Moreno and M Pellaton (both LTF) for helpful discussions. We thank our former colleague S Kang for his contributions to the early phases of the work.

References

[1] Keeler J 2010 *Understanding NMR Spectroscopy* 2nd edn (Chichester: (Wiley)
[2] Budker D and Romalis M 2007 *Nat. Phys.* **3** 227
[3] Vanier J and Audoin C 1989 *The Quantum Physics of Atomic Frequency Standards* (Bristol: Adam Hilger)
[4] Camparo J 2007 *Phys. Today* **60** 33
[5] Julsgaard B, Kozhekin A and Polzik E S 2001 *Nature* **413** 400
[6] Knappe S 2007 Emerging topics: MEMS atomic clocks *Comprehensive Microsystems* ed Y Gianchandani *et al* vol 3 (Amsterdam: Elsevier) p 571–612
[7] Dupuis R T, Lynch T J and Vaccaro J R 2008 *Proc. IEEE Int. Frequency Control Symp.* ed B Jadusliwer *(Honolulu, Hawaii, USA, 19–21 May 2008)* pp 655–60
[8] Waller P, Gonzalez S, Binda S, Sesia I, Hidalgo I, Tobias G and Tavella P 2010 *IEEE Trans. Ultrason. Ferroelct. Freq. Control* **57** 738
[9] Chunhao H, Zhiwu C, Yuting L, Li L, Shenghong X, Lingfeng Z and Xianglei W 2013 *Int. J. Navig. Obs.* **2013** 371450
[10] Kuzmich A, Mandel L and Bigelow N P 2000 *Phys. Rev. Lett.* **85** 1594
[11] Budker D, Gawlik W, Kimball D F, Rochester S M, Yashchuk V V and Weis A 2002 *Rev. Mod. Phys.* **74** 1153
[12] Franzen W 1959 *Phys. Rev.* **115** 850
[13] Liberman V and Knize R J 1986 *Phys. Rev.* **34** 5115
[14] Graf M T, Kimball D F, Rochester S M, Kerner K, Wong C and Budker D 2005 *Phys. Rev.* A **72** 23401
[15] Corsini E P, Karaulanov T, Balabas M and Budker D 2013 *Phys. Rev.* A **87** 22901
[16] Horsley A, Du G X, Pellaton M, Affolderbach C, Mileti G and Treutlein P 2013 *Phys. Rev.* A **88** 063407
[17] Budker D, Hollberg L, Kimball D F, Kitching J, Pustelny S and Yashchuk V V 2005 *Phys. Rev.* A **71** 012903
[18] Castagna N and Weis A 2011 *Phys. Rev.* A **84** 053421
Castagna N and Weis A 2012 *Phys. Rev.* A **85** 059907 (erratum)
[19] Scholtes T, Woetzel S, IJsselsteijn R, Schultze V and Meyer H G 2014 *Appl. Phys.* B **117** 211
[20] Castagna N, Bison G, Di Domenico G, Hofer A, Knowles P, Macchione C, Saudan H and Weis A 2009 *Appl. Phys.* B **96** 763
[21] Hahn E L 1950 *Phys. Rev.* **80** 580
[22] Bar-Gill N, Pham L M, Jarmola A, Budker D and Walsworth R L 2013 *Nat. Commun.* **4** 1743
[23] Hodges J S, Yao N Y, Maclaurin D, Rastogi C, Lukin M D and Englund D 2013 *Phys. Rev.* A **87** 032118
[24] Viola L and Lloyd S 1998 *Phys. Rev.* A **58** 4
[25] Shim J H, Niemeyer I, Zhang J and Suter D 2012 *Europhys. Lett.* **99** 4
[26] Hosseini M, Sparkes B M, Campbell G, Lam P K and Buchler B C 2011 *Nat. Commun.* **2** 174
[27] Tittel W, Afzelius M, Chaneliére T, Cone R L, Kröll S, Moiseev S A and Sellars M 2010 *Laser Photon. Rev.* **4** 244–67
[28] Laplane C, Jobez P, Etesse J, Timoney N, Gisin N and Afzelius M 2016 *New J. Phys.* **18** 013006
[29] Wolfowicz G, Maier-Flaig H, Marino R, Ferrier A, Vezin H, Morton J J L and Goldner P 2015 *Phys. Rev. Lett.* **114** 170503
[30] Bandi T, Affolderbach C, Stefanucci C, Merli F, Skrivervik A K and Mileti G 2014 *IEEE Trans. Ultrason. Ferroelectr. Freq. Control* **61** 1769–78
[31] Kang S, Gharavipour M, Gruet F, Affolderbach C and Mileti G 2015 *Proc. Joint Conf. IEEE Int. Frequency Control Symp. & European Frequency and Time Forum (EFTF) (Denver, Colorado, USA, 12–16 April 2015)* pp 800–3
[32] Vanier J and Mandache C 2007 *Appl. Phys.* B **87** 565–93
[33] Oreto P J, Jau Y Y, Post A B, Kuzma N N and Happer W 2004 *Phys. Rev.* A **69** 042716
[34] Robinson H G, Ensberg E S and Dehmelt H G 1958 *Bull. Am. Phys. Soc.* **3** 9
[35] Bouchiat M A and Brossel J 1966 *Phys. Rev.* **147** 41
[36] Bandi T, Affolderbach C and Mileti G 2012 *J. Appl. Phys.* **111** 124906
[37] Vanier J, Simard J F and Boulanger J S 1974 *Phys. Rev.* A **9** 1031
[38] Franz F A and Lüsher E 1964 *Phys. Rev.* **135** A582
[39] Franz F A 1965 *Phys. Rev.* **139** A603
[40] Carr H Y and Purcell E M 1954 *Phys. Rev.* **94** 630–8

[41] Torrey H C 1956 *Phys. Rev.* **104** 563–5
[42] Risley A, Jarvis S Jr and Vanier J 1980 *J. Appl. Phys.* **51** 4571
[43] Dicke R H 1953 *Phys. Rev.* **89** 472
[44] Stefanucci C, Bandi T, Merli F, Pellaton M, Affolderbach C, Mileti G and Skrivervik A K 2012 *Rev. Sci. Instrum.* **83** 104706
[45] Gruet F, Pellaton M, Affolderbach C, Bandi T, Matthey R and Mileti G 2012 *Proc. Int. Conf. on Space Optics (ICSO) (Ajaccio, Corsica, 9–12 October 2012)* no 48
[46] Calosso C E, Micalizio S, Godone A, Bertacco E K and Levi F 2007 *IEEE Trans. Ultrason. Ferroelectr. Freq. Control* **54** 1731
[47] Gharavipour M, Affolderbach C, Kang S, Bandi T, Gruet F, Pellaton M and Mileti G 2016 *J. Phys.: Conf. Ser.* **723** 012006
[48] Ramsey N 1956 *Molecular Beams* (Oxford: Oxford University Press)
[49] Micalizio S, Godone A, Levi F and Calosso C 2009 *Phys. Rev.* A **79** 013403
[50] Kang S, Gharavipour M, Affolderbach C, Gruet F and Mileti G 2015 *J. Appl. Phys.* **117** 104510
[51] Kang S, Gharavipour M, Affolderbach C and Mileti G 2015 *Electron. Lett.* **51** 1767–9
[52] Affolderbach C, Du G, Bandi T, Horsley A, Treutlein P and Mileti G 2015 *IEEE Trans. Instrum. Meas.* **64** 3629–37
[53] Ardavan A, Rival O, Morton J J L, Blundell S J, Tyryshkin A M, Timco G A and Winpenny R E P 2007 *Phys. Rev. Lett.* **98** 057201
[54] Maineult W, Deutsch C, Gibble K, Reichel J and Rosenbusch P 2001 *Phys. Rev. Lett.* **109** 020407